IOP PUBLISHING NANOTECHNOLOGY
Nanotechnology **18** (2007) 205704 (5pp) doi:10.1088/0957-4484/18/20/205704

Photoconductivity of single-crystalline selenium nanotubes

Peng Liu[1], **Yurong Ma**[2], **Weiwei Cai**[1], **Zhenzhong Wang**[1], **Jian Wang**[1], **Limin Qi**[2] **and Dongmin Chen**[1,3]

[1] Beijing National Laboratory for Condensed Matter Physics, Institute of Physics, Chinese Academy of Sciences, Beijing 100080, People's Republic of China
[2] State Key Laboratory for Structural Chemistry of Unstable and Stable Species, College of Chemistry, Peking University, Beijing 100871, People's Republic of China

E-mail: dmchen@aphy.iphy.ac.cn

Received 5 February 2007, in final form 19 March 2007
Published 23 April 2007
Online at stacks.iop.org/Nano/18/205704

Abstract
The photoconductivity of single-crystalline selenium nanotubes (SCSNTs) under a range of illumination intensities of a 633 nm laser is examined using a novel two-terminal device arrangement at room temperature. It is found that SCSNTs forms Schottky barriers with W and Au contacts, and the barrier height is a function of the light intensity. In the low-illumination regime below 1.46×10^{-4} μW μm^{-2}, the Au–Se–W hybrid structure exhibits sharp on/off switching behaviour, and the turn-on voltages decrease with increasing illuminating intensities. In the high-illumination regime above 7×10^{-4} μW μm^{-2}, the device exhibits ohmic conductance with a photoconductivity as high as 0.59 Ω cm^{-1}, which is significantly higher than the reported values for carbon and GaN nanotubes. This finding suggests that a SCSNT is potentially a good photo-sensor material as well as a very effective solar cell material.

(Some figures in this article are in colour only in the electronic version)

1. Introduction

As an important elemental semiconductor, selenium shows a variety of interesting properties, such as high photoconductivity, nonlinear optical response, and commercial applications in photovoltaic cells, rectifiers, photographic exposure meters, and xerography. Like other photonic semiconductors [1–4], when the dimension and sizes are reduced, a selenium nanostructure is expected to show some quantum-size effects that might offer new or improved photonic applications. In recent years, new synthetic methods for the fabrication of one-dimensional (1D) selenium nanostructures have been successfully developed [5, 6]. So far, however, there have been very limited reports on the physical properties of the nanostructure of Se, especially as an electrical or photonic device. Here we report on a detailed study of the photoconductance of trigonal selenium nanotubes fabricated by a unique, facile and large-scale synthesis method. Extending the scanning tunnelling microscopy (STM) stepper techniques [7], we have successfully developed a novel approach for making clean electrical contacts to individual Se nanotubes to form two-terminal devices for our transport measurements. This versatile technique avoids contact problems often encountered in lithographically patterned devices due to contamination or damage from energetic electron or ion beams. The device made using the present technique forms reliable Schottky barriers at the semiconductor–metal contacts and a back-to-back Schottky diode device. Together with the photo-excitation of the carrier under different light intensities, this type of device exhibits I–V characteristics suitable for photo-sensor and photo-cell applications.

2. Experimental details

Single-crystalline t-Se nanotubes were synthesized by the dismutation of Na_2SeSO_3 under acidic conditions in micellar solutions of the surfactant poly(oxyethylene) dodecyl ether $C_{12}E_{23}$, which is a non-ionic surfactant with a low critical micelle concentration in aqueous solution (typically

[3] Author to whom any correspondence should be addressed.

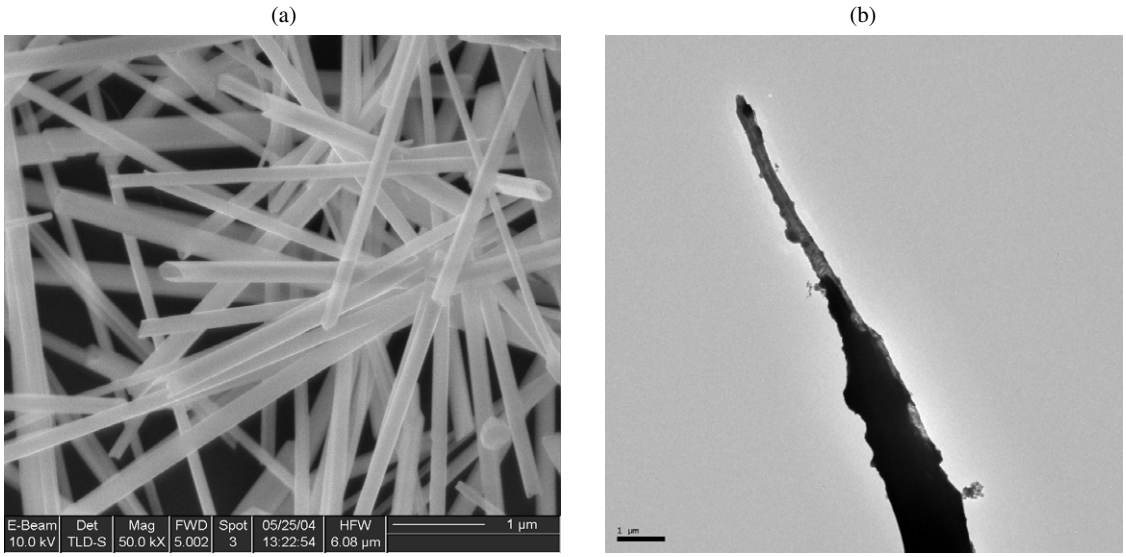

Figure 1. (a) SEM image of single-crystalline Se nanotubes as synthesized; (b) TEM image of an SCSNT attached to a tungsten tip.

4×10^{-5}–2×10^{-4} M) [6]. Figure 1 shows a scanning electron microscope (SEM) image of the t-Se nanotubes. The nanotubes' diameters typically range from 80 to 300 nm and lengths range from several micrometres to more than 100 μm. The tubes have a well-facetted prism morphology with a relatively uniform wall thickness (30–50 nm) and pseudo-hexagonal or pseudo-triangular cross sections. XRD measurements (data not shown) further confirm that the t-Se nanotubes have single-crystal structure with {110} planes on the sides [6].

To perform electrical transport measurements on a single nanotube, we extract an individual tube from the solution by means of dielectrophoresis (DEP). We prepared a sharp tungsten tip by electrochemical etching in a KOH solution of 5 mol l^{-1} [8], followed by chemical etching with dilute HF solution to remove oxidized layers [9]. As illustrated in figure 2(a), the tungsten tip is positioned above a metal electrode (a Au film of a few hundreds of nanometres thick deposited on silicon dioxide substrate) via a high-precision mechanical stage. The apex of a tungsten tip was illuminated by a light-emitting diode (LED) and monitored by a charge-coupled device (CCD) camera in real-time. The tip-facing-tip image in the upper-right of figure 2(a) is the CCD image (with 100 times magnification). From this image, we can estimate that the distance between the tip apex and electrode was about 30 μm. After fixing the tip at this position, we dropped a nanotube solution onto the apex part, and turned on the function generator to generate an ac electrical field. In this process, nanotubes and nanoparticles with a longer dimension having a larger dipole moment are attracted and aligned to the tip sooner than small particles, such as impurities[4]. Figure 1(b) shows a typical image of an SCSNT attached to the tip using this DEP process.

[4] In a nonuniform electric field, the DEP force can be expressed by $F_{\mathrm{DEP}} = 2\pi a^3 \varepsilon_{\mathrm{m}} \mathrm{Re}[\varepsilon_{\mathrm{p}}^* - \varepsilon_{\mathrm{m}}^*/\varepsilon_{\mathrm{p}}^* + 2\varepsilon_{\mathrm{m}}^*]\nabla|E|^2$, where a is the longest dimension of the particle, ε_{m} is the dielectric constant of the medium, ε_{p} is the dielectric constant of the particle, and E is the electric field. When we set the ac voltage $V_{\mathrm{PP}} = 15$ V and frequency $f = 1$ MHz; the maximum electric field was about 2.5×10^5 Vm^{-1}. See [10].

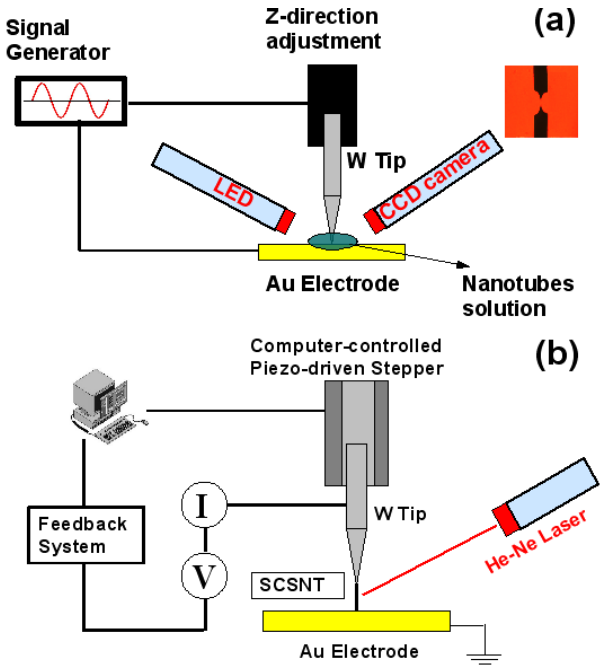

Figure 2. Schematics of (a) dielectrophoresis apparatus used to attach single SCSNT to a metal tip and (b) a single SCSNT two-terminal device arrangement for photoconductivity measurement.

Our two-terminal transport measurement system is shown in figure 2(b), where the nanotube forms one contact with the tip and the other with the Au electrode. A computer-controlled piezo stepper is used to move the tip and nanotube towards the Au electrode in 20 nm steps and at about 20 steps per second [7]. A feedback circuit similar to a scanning tunnelling microscope servo system is used to promptly hold the tip position when a current is detected as a result of the contact between the nanotube and the Au electrode. This method leads to reproducible and controllable contacts and avoids the

oxidation and contamination problems often encountered in the conventional patterned electrode using the lithographical technique.

3. Results and discussion

For photoconductivity measurements, we illuminate the SCSNT with a He–Ne laser ($\lambda = 633$ nm), and the illumination intensity was precisely controlled by two polarizers. One polarizer is parallel to the laser's polarized axis while the other is rotated with respect to the first polarizer to yield the desired light throughput. The laser spot was about 650 μm in diameter and its maximum power was 2 mW in the central part. Assuming a Gaussian distribution of the laser beam and neglecting the scattering from the SCSNT, we estimate that the maximum area power near the centre of the SCSNT was about 60×10^{-4} μW μm^{-2}.

We first measured the dark current using an aluminium foil to shield the ambient light. As shown in the black curve in figure 3(a), under dark conditions the I–V exhibits a gap of 2.24 eV, with a characteristic of two back-to-back Schottky diodes in the W–Se–Au structure. Reverse bias break-down occurs at -0.99 and $+1.25$ V, respectively. Note that the gain of the current preamplifier was set to 10^8, so that the current saturates at ± 100 nA.

The photocondutance for various illumination intensities is shown in figures 3(a)–(c). From 0.018×10^{-4} to 1.46×10^{-4} μW μm^{-2} illumination (figure 3(a)), the I–V spectra continues to show a reverse bias break-through character at both positive and negative biases, but the gap reduces as the photo power increases, suggesting a reduction in the Schottky barrier heights at the nanotube–metal contacts. Note that there is slight asymmetry on the barrier height at these contacts, which can be attributed to the difference in the work-function between the W tip and the Au electrode. When the illumination power rises to between 1.5×10^{-4} and 5.7×10^{-4} μW μm^{-2}, the sharp break-down characteristics of the I–V curves are now replaced by reverse leakage current for either biases, as shown in figure 3(b). Finally, when the illumination power exceeds 7×10^{-4} μW μm^{-2}, the $I(V)$ curves show ohmic behaviour (figure 3(c)). Beyond 25×10^{-4} μW μm^{-2} photo power, the slope of the I–V curve does not change any further, indicating that carrier saturation is reached.

Trigonal selenium is generally accepted as a p-type extrinsic semiconductor, and conduction occurs due to valence band hole transport [11]. Despite the fact that trigonal selenium has a band gap of about 1.6 eV, the room-temperature dark conductivity is usually in the range 10^{-6}–10^{-5} Ω cm^{-1}. Thermoelectric power measurements indicate that at room temperature the majority carriers' concentration is about 10^{13} cm^{-3} [12]. The bulk material electron work-functions of W, Se, and Au are 4.55, 5.9 and 5.1 eV, respectively. Under equilibrium conditions at zero bias, metal–semiconductor (MS) contact and charge transfer cause the band bending near the contacts and Schottky barrier formation as illustrated in figure 4(a), resulting in a back-to-back diode device of figure 4(b). When a voltage is applied across the two MS contacts, one diode is forward biased while the other is reverse biased, as shown in figures 4(c) and (d). For example, when a positive voltage is applied to the W tip, a W–Se Schottky

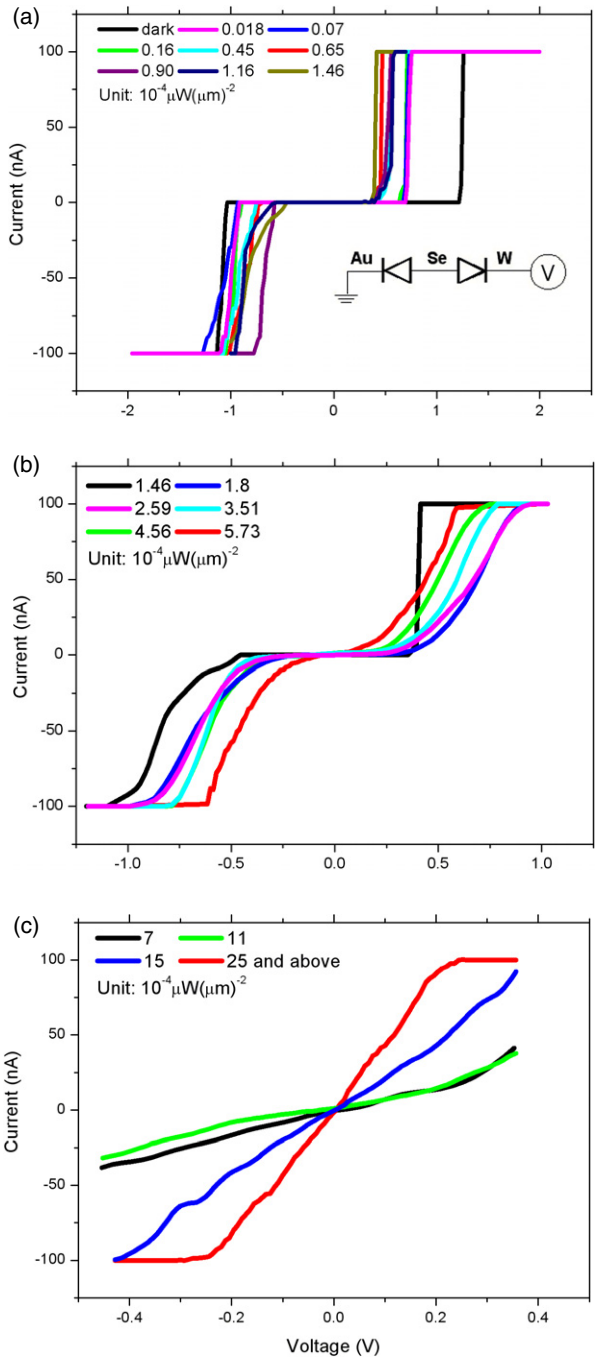

Figure 3. $I(V)$ characteristics of SCSNT under different illumination intensities. The inset shows an equivalent device model of two back-to-back Schottky barrier diodes.

junction is reverse biased while a Au–Se junction is forward biased. In the low-bias regime (0.99 V $> V > -1.25$ V), the circuit is in an off-state. The applied voltage on the W tip $V_A = V_{W-Se} + V_{Au-Se}$. When V_A equates $V_{Flat-Band}$ [13], most of V_A (positive biased, for example) is applied to the W–Se MS junction. When V_A is raised to $V_{Breakdown} = 1.25$ V in dark conditions, reverse avalanche breakdown occurrs in the W–Se junction [13], and there is a rapid rise in the current. The same happens to the Au–Se junction for negative polarity, but the turn-on voltage is slightly different due to the variation in the difference in work-function.

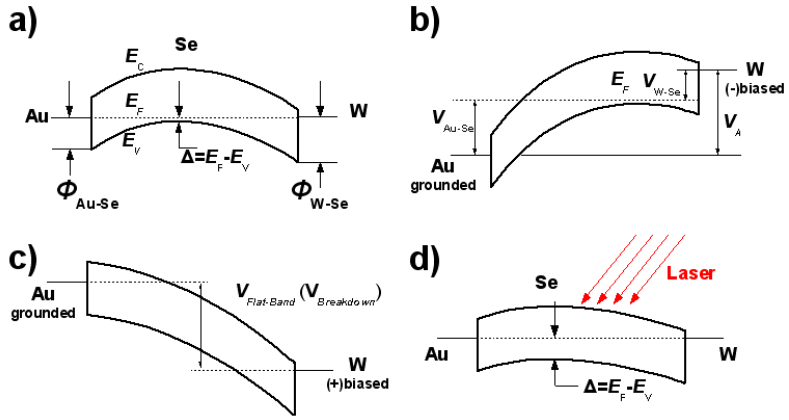

Figure 4. Energy band diagram of Au–Se–W device (a) in equilibrium state with zero bias and under dark conditions; (b) under the low-bias condition, showing bend bending; (c) under the high-bias condition, showing reverse junction breakdown; and (d) under light illumination which reduces the barrier heights.

Under illumination, photo-generated carrier will raise the Fermi level in the Se nanotube and hence lower the Schottky barriers at the MS contacts. This results in a lower switch-on bias voltage, as shown in figure 3(a). As the barrier height lowers further with increasing illumination intensity, the reverse breakdown voltage was not enough to induce the avalanche process, so the current rises slowly instead (figure 3(b)). Since most of the bias voltage falls at the reverse bias junction, the switch-on points are the measure of the respective Schottky barrier heights. Figure 5(a) plots the change in the Schottky barrier heights as a function of illumination intensity. It shows that the Schottky barriers decreased continuously with increasing illumination intensity but the difference between the Schoottky barrier heights is almost constant at ∼0.26 eV (within the measurement error bars) before reaching carrier saturation. It should be noted that the illumination intensity values are somewhat over-estimated, because we have not taken into account the effects of incident light scattering from the Se nanotube.

When the illumination intensity equals or exceeds 7×10^{-4} μW μm^{-2}, both Schottky barriers nearly disappear and the conductance exhibits ohmic behaviour, as shown in figure 3(c). Finally, when the illumination power reaches 25×10^{-4} μW μm^{-2} and above, the conductance saturates. Figure 5(b) shows the conductance as a function of the illumination intensity, where $\sigma = LI/VS$ is extracted from the linear fits of the data in figure 3(a) with $L = 10$ μm, $\varphi = 320$ nm, and wall thickness $= 50$ nm. Note that $R = R_{\mathrm{Au-Se}} + R_{\mathrm{W-Se}} + R_{\mathrm{se}}$, so saturation might indicate that the contact resistances are the limiting factor and the photoconductance of a Se nanotube could be much higher than 0.59 $(\Omega\ \mathrm{cm})^{-1}$.

The dependence of photoconductivity on the illumination intensity is determined mainly by the recombination and trapping of the electron–hole pairs within solid materials, and the rate of such a recombination and trapping for selenium has been shown to depend strongly on temperature [5]. Both light adsorption and resistive heating can raise the sample temperature and affect the conductance. In our study, however, the illumination power was so low that its heating effect should not have a significant influence on the photoconductivity.

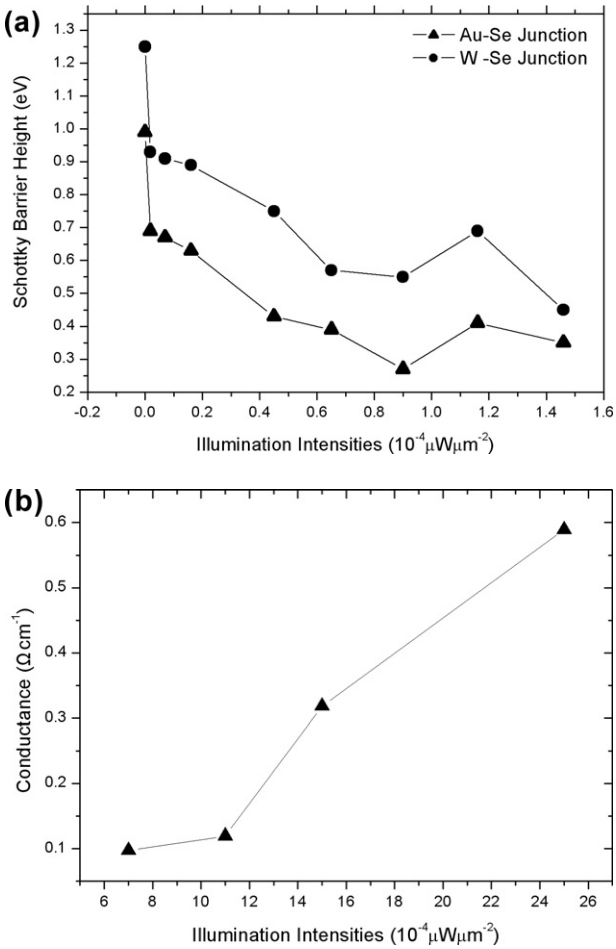

Figure 5. (a) Schottky barrier heights of Au–Se and W–Se contact under low-power illumination; (b) photoconductivity of Au–Se–W device under under low-power illumination.

Previous work on the phtoconductivity of selenium focused on amorphous selenium, liquid selenium and hexagonal metallic selenium film or bulk materials [14]. A recent experiment on t-Se nanowire yields $\sigma = 12.4$ $(\Omega\ \mathrm{cm})^{-1}$ with $\sim\mu$W μm^{-2}

illumination intensity [5]. Our results indicate that, with four-orders-of-magnitude lower illumination intensities, $\sim 10^{-4}$ μW μm^{-2}, the SCSNTs exhibit a much higher photoconductivity of 0.59 $(\Omega\ \mathrm{cm})^{-1}$. This also compares favourably with other nanomaterials, such as single-walled carbon nanotubes (kW cm^{-2}, 0.38 $(\Omega\ \mathrm{cm})^{-1}$) [15] and GaN nanowires (15 W cm^{-2}, 0.026 $(\Omega\ \mathrm{cm})^{-1}$) [16].

An increase in the conductivity can come from an increase in carrier density or mobility, or both. The increase in photoconductivity in single-crystal materials is due primarily to an increase in carrier density. The cut-off excitation wavelength according to the t-Se band gap (1.6 eV) is $\sim$770 nm. Our laser wavelength, 633 nm, is sufficient to excite abundant carriers via photo-absorption, band–band transition, and valence-band to acceptor and donor to conduction-band transitions. On the other hand, photoconduction depends strongly on the efficiency of the charge separation. Any electron–hole pair that recombines within the bulk or the surface via surface states of the materials is a major loss mechanism for photo-generated carriers. Thus a small density of recombination centres is preferred. Surface traps, however, can be beneficial for charge–carrier separation, as they 'store' the charge–carrier and hence reduce the recombination rate. In nanostructures, duo to a high surface-to-volume ratio, there exist much more surface states and defects than bulk or film materials. These defects could induce more defect-localized states which might act as trapping, releasing and recombination centres of minority carriers, i.e. electrons, in selenium crystal. Consequently, mechanisms for increasing photoconduction by trapping as well as for reducing photoconduction due to carrier releasing and recombination are both enhanced in nano-scale structures, though their relative contributions vary with different materials or structures. It seems that in SCSNT the former dominates. The exceptionally high photoconductivity of SCSNT might find superior applications such as photo-sensor and photo-cell materials.

4. Conclusions

In conclusion, we have measured the photoconductivity of SCSNT using a two-terminal measurement system under different illumination intensities at room temperature. In the low-illumination regime below 1.46×10^{-4} μW μm^{-2}, the Au–Se–W hybrid structure exhibits sharp switch-on and switch-off behaviour. Also, with an increase in illumination intensities, the turn-on voltage values decrease. This conclusion suggests that SCSNT is potentially a good photo-sensor material. On the other hand, in the high-illumination regime above 7×10^{-4} μW μm^{-2}, due to a high photo-generated carrier density, SCSNT exhibits exceptional high photoconductivity. This indicates that SCSNT could also be a very effective solar cell material. Further study of the spectral dependence of the photo-conductivity of SCSNT is clearly of great interest.

Acknowledgments

The authors would like to thank Zhi Xu and Xuedong Bai for their kind help with TEM, and Fei Pang for his kind help in software programming. Financial support for this work via a grant (no. 50518002) from NSFC-HKRGC (National Natural Science Foundation of China-Hong Kong Research Grants Council) is gratefully acknowledged.

References

[1] Frank S, Poncharal P, Wang Z L and de Heer W A 1998 *Science* **280** 1744
[2] Hu J, Odom T W and Lieber C 1999 *Acc. Chem. Res.* **32** 435
[3] Wang Z L 2000 *Adv. Mater.* **12** 1295
[4] Xia Y, Yang P, Sun Y, Wu Y, Mayers B, Gates B, Yin Y, Kim F and Yan Y 2003 *Adv. Mater.* **15** 353
[5] Gates B, Mayers B, Cattle B and Xia Y 2002 *Adv. Funct. Mater.* **12** 219
[6] Ma Y, Qi L, Ma J and Cheng H 2004 *Adv. Mater.* **16** 1023
[7] Okamoto H and Chen D M 2001 *Rev. Sci. Instrum.* **72** 4398
[8] Dremov V V, Makarenko V A, Shapoval S Y, Trofimov O V, Beshenkov V G and Khodos I I 1994 *Nanobiology* **3** 83
[9] Fasth J E, Loberg B and Norden H 1967 *J. Sci. Instrum.* **44** 1044
[10] Lee H W, Kim S H and Kwak Y K 2005 *Rev. Sci. Instrum.* **76** 046108
[11] Mort J 1967 *Phys. Rev. Lett.* **18** 540
[12] Abdullayev G B, Dzhalilov N Z and Aliyev G M 1966 *Phys. Lett.* **23** 217
[13] Grundmann M 2006 *The Physics of Semiconductors* (Berlin: Springer) p 492
[14] Moss T S 1952 *Photoconductivity in the Elements* (London: Butterworths) pp 185–203
[15] Freitag M, Martin Y, Misewich J A, Martel R and Avouris Ph 2003 *Nano Lett.* **3** 1067
[16] Calarco R, Marso M, Richter T, Aykanat A I, Meijers R, Hart A v d, Stoica T and Luth H 2005 *Nano Lett.* **5** 981